ORIGINAL ARTICLE

Flexural performance of concrete beams reinforced with steel–FRP composite bars

Wenjie Ge[1,2] · Yanming Wang[1] · Ashraf Ashour[3] · Weigang Lu[2] · Dafu Cao[1]

Abstract

Flexural performance of concrete beams reinforced with steel–FRP composite bar (SFCB) was investigated in this paper. Eight concrete beams reinforced with different bar types, namely one specimen reinforced with steel bars, one with fiber-reinforced polymer (FRP) bars and four with SFCBs, while the last two with hybrid FRP/steel bars, were tested to failure. Test results showed that SFCB/hybrid reinforced specimens exhibited improved stiffness, reduced crack width and larger bending capacity compared with FRP-reinforced specimen. According to compatibility of strains, materials' constitutive relationships and equilibrium of forces, two balanced situations, three different failure modes and balanced reinforcement ratios as well as analytical technique for predicting the whole loading process are developed. Simplified formulas for effective moment of inertia and crack width are also proposed. The predicted results are closely correlated with the test results, confirming the validity of the proposed formulas for practical use.

Keywords Steel–FRP composite bar (SFCB) · Concrete beams · Flexural behavior · Capacity for bending · Deflection · Crack

1 Introduction

The use of FRP bars as an alternative reinforcement in concrete structures has shown to be a valid way to overcome the durability issues of steel-reinforced concrete structures, resulting from the corrosion of steel reinforcement. Over the past two decades, the performance of FRP-reinforced concrete structures has received significant attentions, and this new reinforced system is being widely used in marine structures, hydraulic structures, high-speed railway and subway structures. Masmoudi [1] experimentally and theoretically investigated the effect of FRP reinforcement ratio on cracking, deflection, bending capacity and modes of failure of concrete beams. Grace [2] carried out the experimental study on the mechanical behavior of reinforced concrete

beams strengthened by FRP laminates. Pecce [3] discussed the structural behavior, such as curvature, deflection, and crack spacing and width, of concrete beams reinforced with glass FRP bars and analyzed verifications at ultimate and serviceability conditions. Aiello [4] investigated the deformability of concrete flexural members reinforced with FRP rebars. Gravina [5] conducted comparative tests on simply supported and continuous concrete beams reinforced with FRP bars to predict the bending moment distribution. Xue [6] proposed a calculation method for deflections of concrete beams reinforced with FRP rebars. Qi [7] conducted an experimental study on cracking patterns, load–deflection response, load–moment relationship, internal force redistribution and ultimate load of continuous beams reinforced with FRP rebars. Tu [8] conducted an experimental study on simply supported beams reinforced with bonded AFRP tendons, and an effective calculation method for the ultimate load-carrying capacities was derived. Skuturna [9] studied the design methods for calculating the load-carrying capacity of reinforced concrete elements in flexure strengthened with external FRP reinforcement. Lapko [10] reported that much lesser cross-sectional stiffness of basalt BFRP bars produces higher deflections and crack widths compared to the beams reinforced with steel bars of the same cross

✉ Wenjie Ge
gewj@yzu.edu.cn

1 College of Civil Science and Engineering, Yangzhou University, Yangzhou 225127, China

2 College of Hydraulic Science and Engineering, Yangzhou University, Yangzhou 225127, China

3 Department of Civil Engineering, University of Bradford, Bradford BD71DP, UK

section. Zhou [11] investigated the in-plane seismic behavior of eight unreinforced masonry walls before and after being retrofitted by BFRP.

Mahroug [12] showed that continuously supported BFRP-reinforced concrete slabs exhibited larger deflections, wider cracks and brittle failure compared with the counterpart reinforced with steel. Such behavior is attributed to the fact that FRP reinforcing bars exhibit a linear elastic stress–strain relationship up to failure without any yielding, causing brittle failure without enough warning to RC structures user. Therefore, few suggestions were recently proposed to improve the ductility of FRP-reinforced concrete members.

A hybrid system consisting of both FRP and steel reinforcement was introduced to improve reinforced concrete element ductility and durability [13–21]. In such reinforcement system, FRP reinforcement is located in the outer layer, whereas steel bars are embedded more deeply, achieving larger cover concrete, combining the advantages of FRP and steel reinforcement simultaneously by improving durability and ductility as well as reducing deflection and crack width. Lau [13] proposed that steel longitudinal reinforcement should be added to form a hybrid FRPRC beam to improve its ductility. Huang [14] conducted an experimental and theoretical study on the mechanical behaviors of steel–GFRP-reinforced concrete beams. Ge [15, 16] investigated the flexural behavior of hybrid FRP/steel-reinforced concrete beams and ECC–concrete composite beams. The test results showed that the ductility of hybrid reinforced composite beams is higher than that of traditional RC beams and formulas for cracking, yield and ultimate moments as well as deflections of hybrid reinforced beams are developed. Kara [17] presented a numerical method for estimating the curvature, deflection and moment capacity of hybrid FRP/steel-reinforced concrete beams. Refai [18] reported the structural performance of concrete beams reinforced with steel and GFRP hybrid reinforcement. Yoo [19] investigated the flexural behavior of UHPFRC beams reinforced with GFRP rebars and steel/GFRP hybrid reinforcements. Sun [20] conducted an experimental study on the flexural behavior of concrete beams reinforced with bundled hybrid steel/FRP bars. Maranan [21] investigated the flexural behavior of geopolymer concrete beams reinforced with a hybrid GFRP and steel bars.

Wu et al. [22] recently introduced a newly developed steel–FRP composite bar (SFCB), composed of inner steel bar wrapped by FRP, combining the advantages of the two materials. SFCBs exhibit high strength, good ductility, high elastic modulus, stable secondary stiffness and excellent corrosion resistance. Uniaxial static and cyclic tensile tests of SFCB showed a bilinear stress–strain relationship before FRP rupture. After the inner steel yielded, SFCB displayed a stable post-yielding stiffness. Few investigations showed the effectiveness of SFCB as structural reinforcement for

concrete structures [23, 24]. However, further experimental and computational investigations of structural elements reinforced with SFCBs are essential to better understand their structural behavior and to encourage their use in real structures.

In this paper, static flexural experiments of SFCB, steel, FRP and hybrid RC beams were conducted and compared. The effect of reinforcement form and ratio on the bending capacity, crack width and deflection of RC specimens was studied. Theoretical analysis based on strain compatibility, realistic constitutive relationships and forces equilibrium is also conducted to predict the failure modes, bending capacity, crack width and deflections. Taking the properties of SFCB materials into consideration, modified formulas for the crack width and effective moment of inertia of SFCB RC flexural components are also proposed.

2 Experimental design

2.1 Mechanical performance of material

2.1.1 Concrete

The main concrete ingredients were Portland cement (CEM 42.5), medium sand of grain diameter 0.35–0.5 mm, gravel of maximum size 15 mm and tap water. The mass ratio of water, cement, sand and gravel was 0.39:1.0:1.29:2.88, i.e., 168, 432, 558 and 1242 kg, respectively, for one cubic meter of concrete. The concrete compressive test was conducted at the same time as the flexural experiment of RC beams. The mean compressive strength $f_{cu, mv}$ of concrete obtained from testing three $150 \times 150 \times 150$ mm [25] cubes was 43.85 MPa. The modulus of elasticity E_c $(= 10^2/(2.2 + 34.7/f_{cu}))$, compressive strength f_c $(= 0.88\alpha_{c1}\alpha_{c2}f_{cu})$ and tensile strength f_t $(= 0.348\alpha_{c2}f_{cu}^{0.55})$ are 33.43 GPa, 28.65 MPa and 2.80 MPa, respectively [26], where α_{c1} is the strength ratio of concrete prism to concrete cube and α_{c2} is the brittleness reduction coefficient of high-strength concrete.

2.1.2 Longitudinal reinforcements

Five different types of longitudinal reinforcements were used, namely steel, basalt FRP (BFRP) and three SFCBs with different arrangements. Table 1 and Fig. 1a present details of the reinforcements used, where d and d_s are the full and steel diameters, OFT represents the out-wrapping fiber type, t_f is the thickness of outer FRP material, d_r and s_r are the depth and spacing of ribbed ribs, respectively. All reinforcing bars were of 12 mm diameter. Reinforcing bars A and E were fully made of steel and BFRP, respectively, whereas the other three bars had an inner steel core of

Table 1 Details of longitudinal reinforcement

No.	d (mm)	d_s (mm)	OFT	t_f (mm)	d_r (mm)	s_r (mm)
A	12	12	–	0	1.2	8.0
B	12	6	Basalt FRP	3	1.5	10.0
C	12	8	Basalt FRP	2	1.5	10.0
D	12	6	Glass FRP	3	1.5	10.0
E	12	0	Basalt FRP	6	1.5	10.0

Fig. 1 Tested longitudinal reinforcements

(a) Reinforcements

(b) Anchorage of FRP/SFCB reinforcement
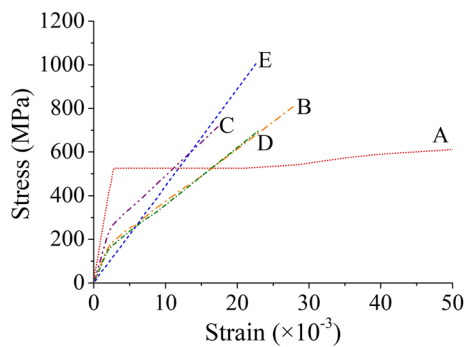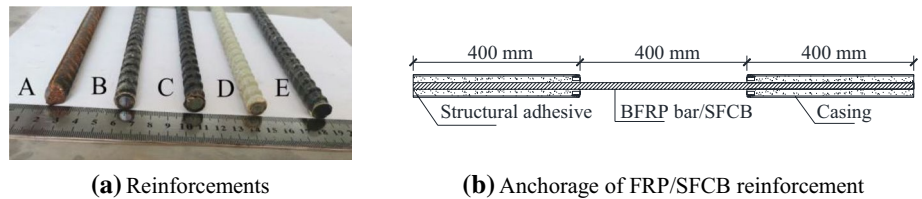
Fig. 2 Tensile stress–strain curves of tested bars

Table 2 Mechanical performance of tested bars

No.	f_y (MPa)	E_I (GPa)	f_u (MPa)	E_{II} (GPa)
A	524.0	198.0	642.0	0.0
B	150.2	72.3	798.5	25.7
C	230.0	112.9	704.3	30.6
D	150.1	67.3	688.9	25.8
E	–	46.1	1002.3	–

diameter d_s, externally wrapped with FRP layer of thickness t_f achieving the full diameter d.

Tensile properties of FRP and SFCB reinforcements were obtained by testing three specimens for each type [27]. The total length, anchorage and free length of the specimen were 1200, 400 and 400 mm, respectively, as shown in Fig. 1b. Figure 2 and Table 2 present the tensile stress–strain curves and mechanical properties of tested bars, respectively; the values of modulus of elasticity as well as the strengths are the mean values from three test specimens. E_I and E_{II} are the moduli of bars before and after yielding, respectively; f_u and f_y are the ultimate and yield stress of bars, respectively. As

reinforcing bars E are purely made from FRP material, only E_I is measured and presented.

As can be seem from Fig. 2 and Table 2, the three SFCBs, all, exhibit stable secondary stiffness. At the beginning, the load was carried by the outside fiber and inner steel simultaneously; the higher the proportion of inner steel, the higher the elastic modulus E_I and yield strength f_y. The SFCB appeared to yield when its strain is up to about 0.002 (the yield strain of inner steel). This is illustrated by the fact that SFCB had fewer, but stably increasing, stress increments with the same strain increment, which means that SFCB exhibited stable stiffness after inner steel yielded (post-yield stable secondary stiffness). Because the inner steel had already yielded, the load was mainly resisted by the outside fiber. As the load increased, the loading capacity reached its peak when the fiber fractured at the middle part of the specimen [22].

Figure 3 presents the typical failure mode of each type of refinements. In all specimens, failure occurred at the middle region of the specimens, indicating that the end anchorage was effective. The steel–FRP composite bar underwent a threadlike blowout fracture, illustrating that the resin component of SFCB had better coupling performance with fiber [22].

2.1.3 Bond-slip behavior

Standard pullout experiments were conducted to test the bond-slip behavior between the five reinforcing bars and concrete [28]. Figure 4a–c represents the schematic diagram of pullout specimen, pullout setup and bond stress–strain curves, respectively.

Plastic pipes were embedded to reduce the local stress at the load end during testing. The loading was applied by a hydraulic jack and measured by a load sensor; the slip of the
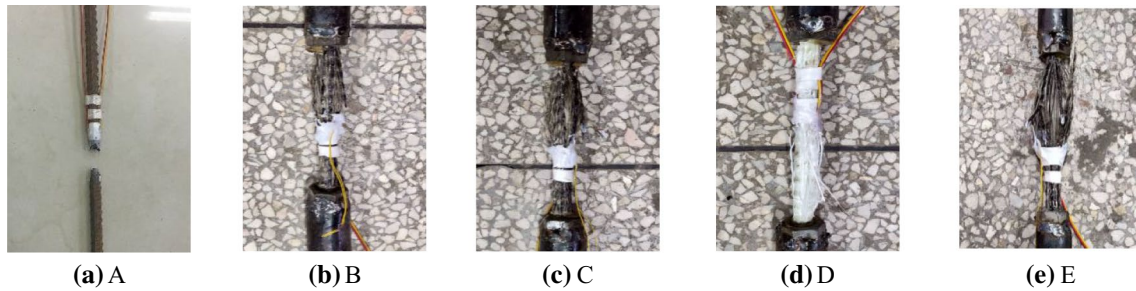
(a) A **(b)** B **(c)** C **(d)** D **(e)** E

Fig. 3 Failure modes of tested bars

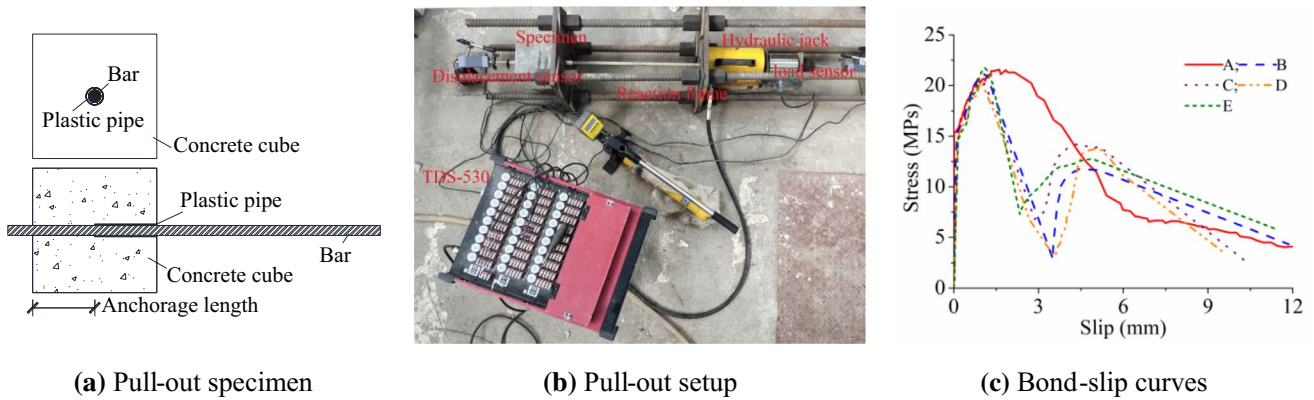**(a)** Pull-out specimen **(b)** Pull-out setup **(c)** Bond-slip curves

Fig. 4 Pullout test

Table 3 Bond properties of reinforcement

Notation	Diameter (mm)	Surface feature	τ (MPa)	τ_i/τ_A	n_a
A	12	Ribbed	20.6	1.00	7.8
B	12	Ribbed	20.9	1.01	9.6
C	12	Ribbed	20.1	0.98	8.8
D	12	Ribbed	20.4	0.99	8.4
E	12	Ribbed	21.4	1.04	11.7

free end was measured by a displacement sensor attached to the bar.

Table 3 presents the bond strengths of each reinforcing bar with concrete, while Fig. 5 shows the tested bond-slip specimens, where the bond strength of concrete and reinforced bars, τ, is the stress corresponding to a bond slip of 1.0 mm [29].

All specimens' anchorage lengths were $5d$ to promote the same failure mode of pullout. As can be seen from Table 3, the bond strength ratio τ_i/τ_A of SFCBs/BFRP bar to steel bar is all approximately equal to 1.0, illustrating that the ribbed SFCBs/BFRP bar has very similar bond strength as ribbed steel bar.

Table 4 presents the anchorage length with respect to the bar diameter, $n_a = L_a/d$, where L_a is the anchorage length, of various reinforced bars. The anchorage length is obtained by considering the balance failure case, where bar pullout and rupture simultaneously occur; $f_u \pi d^2/4 = \tau \pi d L_a$, d is the bar diameter, τ is the bond strength of concrete and reinforced bars, f_u is the tensile strength of the reinforced bars and L_a is the anchorage length of the reinforced bars. Rearranging the above formula, the anchorage length with respect to the bar diameter can be obtained, $n_a = L_a/d = f_u/4\tau$, as presented in Table 4.

2.2 Specimens design and testing program

In total, eight specimens were tested to investigate the flexural performance, one steel RC specimen, one FRP RC specimen, two hybrid steel/FRP RC specimens and the other four SFCB RC specimens. Details of specimens are shown in Table 4, and reinforcement details are presented in Fig. 6. The cross section width is $b = 120$ mm and height is $h = 180$ mm. The height of the centroid of reinforced bars to the cross section extreme tensile fiber is $h_r = 25$ mm, and the effective height of cross section is $h_0 = 175$ mm. ρ represents the practical reinforcement ratio, $\rho = A/(bh_0)$, A is

**Fig. 5** Failure mode of tested bond-slip specimens

(a) Untested specimen

(b) A

(c) B

(d) C

(e) D

(f) E
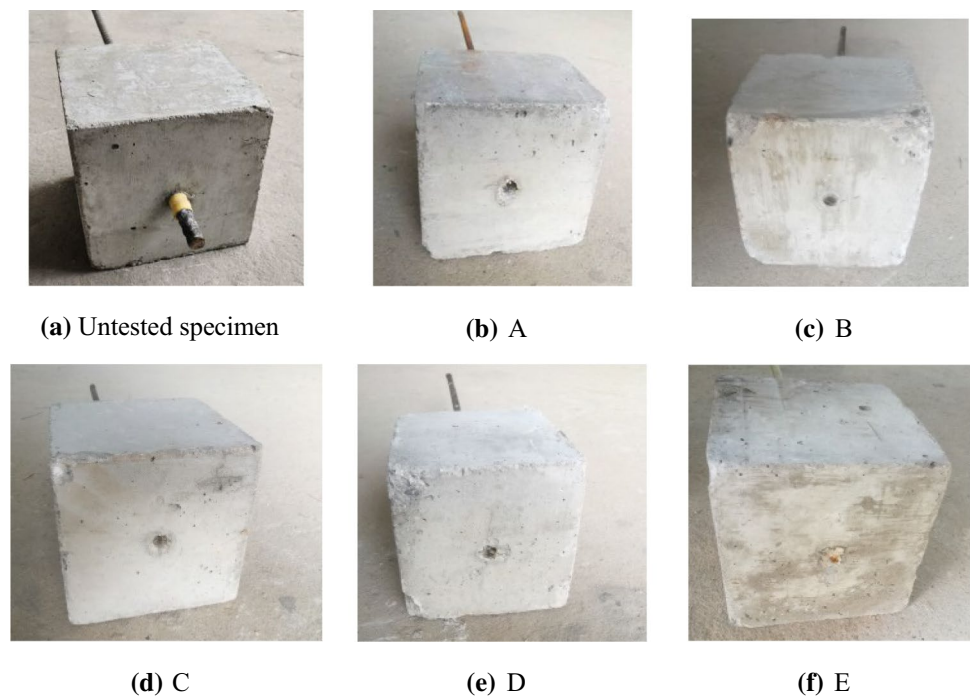
Table 4 Details of designed specimen

No.	Longitudinal reinforcements	Stirrups	Erection bar	ρ (%)	ρ_{nE} (%)	ρ_{nf} (%)	F_u (kN)
BA	2A	Φ8@40	2Φ12	1.22	1.22	1.49	145.1
BB	2E	Φ8@40	2Φ12	1.22	0.28	2.82	226.5
BC	2B	Φ8@40	2Φ12	1.22	0.44	2.25	180.5
BD	3B	Φ8@40	2Φ12	1.82	0.67	3.26	270.7
BE	2C	Φ8@40	2Φ12	1.22	0.69	1.98	159.2
BF	2D	Φ8@40	2Φ12	1.22	0.41	1.94	155.7
BG	2E+A	Φ8@40	2Φ12	1.82	0.89	2.93	299.1
BH	E+A	Φ8@40	2Φ12	1.22	0.75	1.77	185.8

the cross section area of reinforced bars; ρ_{nE} represents the nominal elastic modulus reinforcement ratio, for SFCB RC specimen, $\rho_{nE} = \rho E_I/E_s$, and for FRP/steel hybrid RC specimens, $\rho_{nE} = \rho_s + \rho_f E_f/E_s$; ρ_{ns} represents the nominal strength reinforcement ratio, for SFCB RC specimens, $\rho_{ns} = \rho f_{sfu}/f_y$, and for FRP/steel hybrid RC specimens, $\rho_{ns} = \rho_s + \rho_f f_{fu}/f_y$. F_u represents the tensile capacity of longitudinal reinforcement, for SFCB RC specimens, $F_u = f_{sfu}A_{sf}$, for FRP RC specimens, $F_u = f_{fu}A_f$, for steel RC specimens, $F_u = f_u A_s$ and for hybrid RC specimens, $F_u = f_{fu}A_f + f_u A_s$. A_f and A_s are the cross section areas of FRP and steel reinforcement, respectively. ρ_f and ρ_s are the reinforcement ratio of FRP and steel reinforcement, respectively. f_{fu} and f_{sfu} are the ultimate stress of FRP and SFCB reinforcement, respectively. f_u and f_y are the ultimate and yield stress of steel bars, respectively. E_f, E_s and E_I are the elastic modulus of FRP, steel and SFCB before the yielding of inner steel, respectively.

2.3 Loading and testing program

Figure 7 presents the loading and testing system. The moment was controlled by a distribution beam on the top of the specimen and applied by a hydraulic jack, while its value was tested by a load sensor (measurement resolution 0.10 kN, accuracy ± 0.10 kN) laid on the top of the jack. Electrical resistance strain acquisition instrument TDS-530 was used to capture loading at various stages. Dial indicators (type I, measurement resolution 0.01 mm, accuracy ± 0.02 mm) were located at mid-span, supporting and loading points. Cracks distributed between the pure flexural span were marked, and their widths (at the height the same as the centroid of reinforcement) were measured and recorded at various loading stages by crack width measuring instrument KON-FK(B) (measurement resolution 0.02 mm, accuracy ± 0.02 mm). Dial indicators equidistant (type II,

Fig. 6 Schematic diagram of test specimens
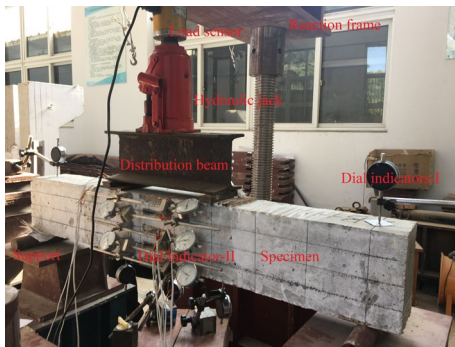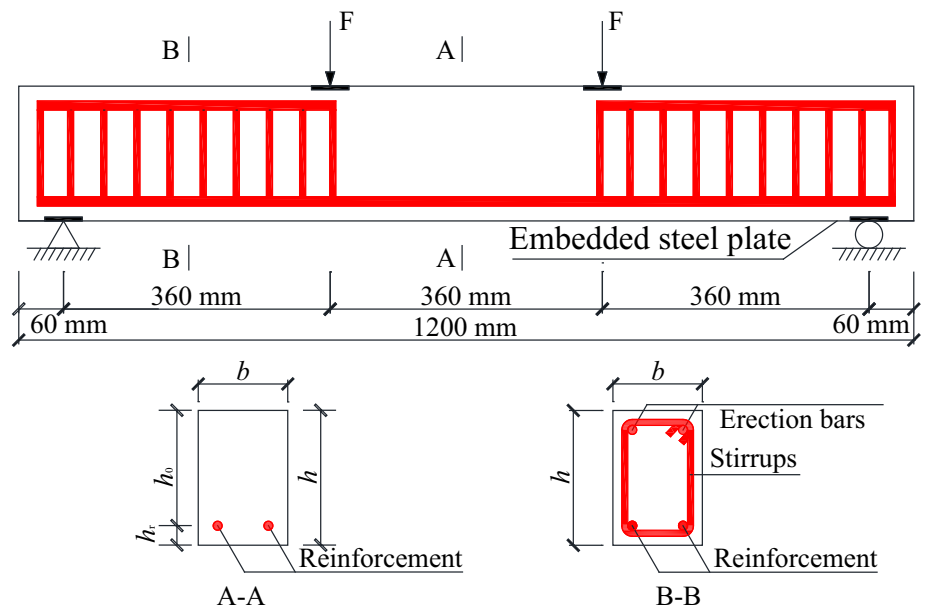
Fig. 7 Loading and testing system

measurement resolution 0.001 mm, accuracy ± 0.003 mm) with 200 mm measurement length along the height direction (10, 45, 90, 135 and 170 mm, respectively) on the side of mid-span cross section were pasted to measure the average concrete strains under various applied loads.

3 Experimental results and analysis

3.1 Distribution of concrete average strain

Figure 8 presents the distribution of concrete average strain along the cross section height at various loading stages, where M_u is the experimental ultimate bending moment.

As observed from Fig. 8, the depths of neutral axis gradually move up with the increase in loading. The average concrete strain along the cross section height is almost a linear distribution, illustrating the validity of the plane section assumption that will be used later in the analytical

development below. The depth of neutral axis of steel-reinforced specimen BA is the smallest, that of FRP-reinforced specimen BB is the largest, whereas that of SFCB/hybrid reinforced specimens is in between, reflecting reinforcing bars' modulus as measured above.

3.2 Moment–deflection curves

Figure 9 presents the moment–deflection curves at mid-span, where d_{lim} is the deflection limit under serviceability state (that is 3.75 mm) [30] for all test specimens.

As observed from Fig. 9, the beams tested display different features, depending on the characteristics of the reinforcement used. For beams reinforced with FRP bars, two distinct stiffnesses are clearly identified, namely before cracking of concrete and after cracking until concrete crushing. On the other hand, the loading process of SFCB/hybrid RC specimens obviously presents three stages: Stage 1: from initial loading until concrete cracking; Stage 2: after concrete cracking to yielding of SFCB reinforcement (inner steel); Stage 3: stable secondary stiffness after yielding until concrete crushing. The beam reinforced with steel bars exhibited similar behavior to that of SFCB/hybrid RC specimens, but after yielding, the beam stiffness was almost flat. The deflections of SFCB/hybrid RC specimens increase gradually with an increase in the applied load after the yielding of SFCB/steel. For steel reinforcement almost fully plastic after yielded, the deflections of steel RC specimens increase dramatically even the load does not increase.

Table 5 presents the comparison of crack, yield and ultimate moments of all specimens, where the yield moment of specimen BA and ultimate moment of specimen BB are taken as control moments: cracking moment
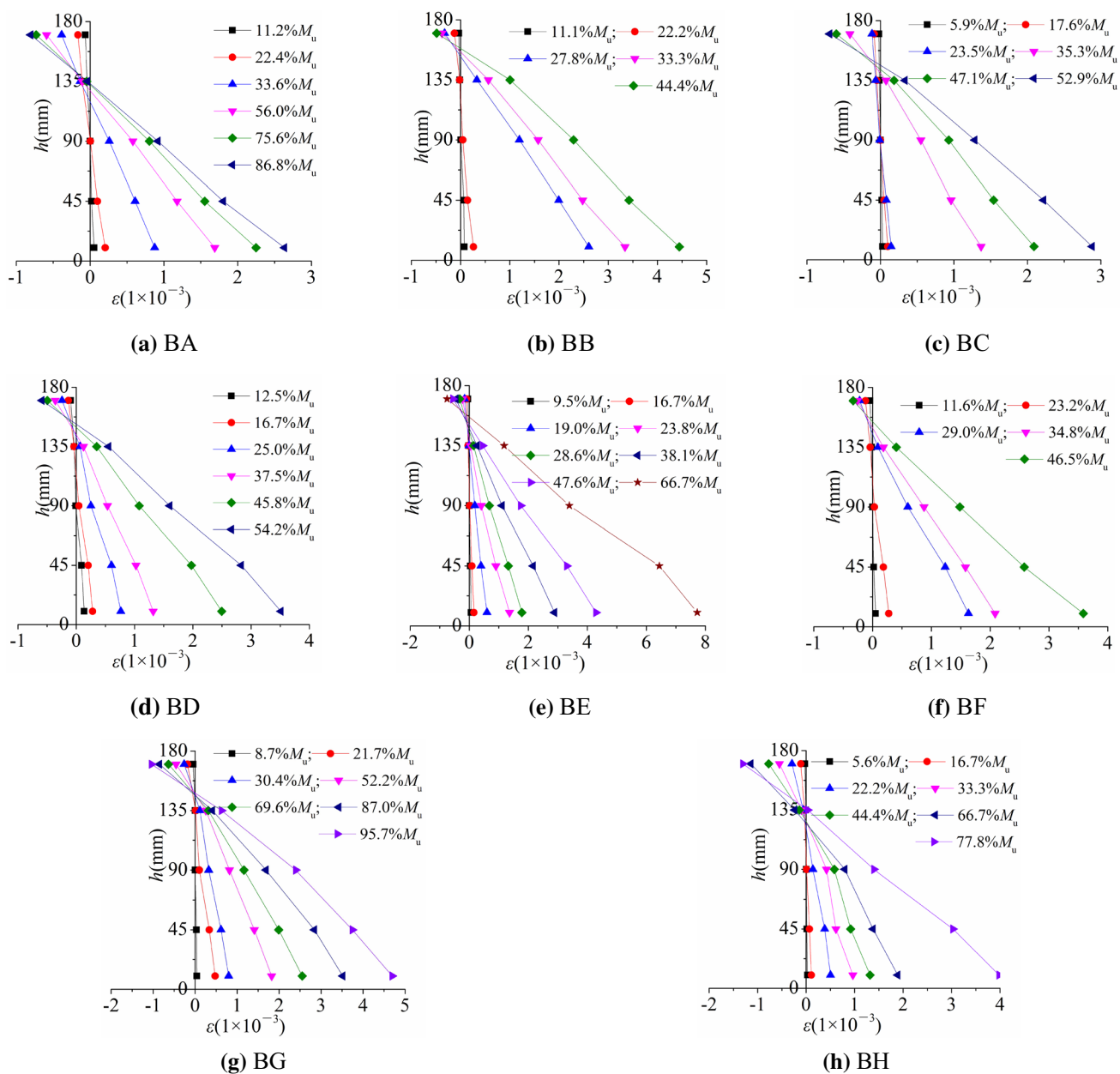
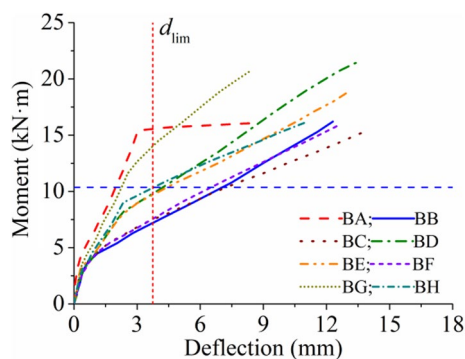**Fig. 8** Distribution of concrete average strain

Fig. 9 Moment–deflection curves

M_{cr} corresponding to the crack of tensile concrete, yield moment M_y corresponding to the yielding of tensile steel or SFCB, and ultimate moment M_u corresponding to the crushing of compressive concrete.

As observed from Table 5, all specimens have similar cracking moment; the yield moments increase with an increase in nominal elastic modulus reinforcement ratio. Ultimate moment increases ($M_{u, BF} = 15.80$ kN m $< M_{u, BE} = 18.90$ kN m) with an increase in the nominal elastic modulus reinforcement ratio ($\rho_{nE, BF} = 0.41\% < \rho_{nE, BE} = 0.69\%$) while specimens

Table 5 Comparison of capacity for bending

| No.	ρ (%)	ρ_{nE} (%)	ρ_{nf} (%)	F_u (kN)	M_{cr} (kN·m)	M_y (kN·m)	M_u (kN·m)	$M_y/M_{y,BA}$ (%)	$M_u/M_{u,BB}$ (%)
BA	1.22	1.22	1.49	145.1	3.22	15.41	16.07	100.00	99.2
BB	1.22	0.28	2.82	226.5	3.15	–	16.20	–	100.0
BC	1.22	0.44	2.25	180.5	3.15	5.40	15.30	35.04	94.4
BD	1.82	0.67	3.26	270.7	3.15	8.00	21.60	51.91	133.3
BE	1.22	0.69	1.98	159.2	3.15	8.10	18.90	52.56	116.7
BF	1.22	0.41	1.94	155.7	3.15	4.50	15.80	29.20	97.5
BG	1.82	0.89	2.93	299.1	3.15	10.80	20.70	70.08	127.8
BH	1.22	0.75	1.77	185.8	3.15	9.00	16.20	58.40	100.0

Table 6 Comparison of deflections and crack widths

No.	ρ (%)	ρ_{nE} (%)	ρ_{nf} (%)	F_u (kN)	M_u (kN m)	$d_{q,BB}$ (mm)	$M_{d,lim}$ (kN m)	$M_{d,lim}/M_u$ (%)	$\omega_{q,BB}$ (mm)	$M_{\omega,lim}$ (kN m)	$M_{\omega,lim}/M_u$ (%)
BA	1.22	1.22	1.49	145.1	16.07	1.98	15.55	96.77	0.13	15.41	95.88
BB	1.22	0.28	2.82	226.5	16.2	7.24	7.20	44.44	0.56	6.94	42.83
BC	1.22	0.44	2.25	180.5	15.3	6.52	7.50	49.02	0.54	8.03	52.50
BD	1.82	0.67	3.26	270.7	21.6	4.23	9.80	45.38	0.32	11.55	53.48
BE	1.22	0.69	1.98	159.2	18.9	4.43	9.70	51.34	0.31	10.52	55.64
BF	1.22	0.41	1.94	155.7	15.8	7.06	7.56	47.83	0.55	7.90	50.03
BG	1.82	0.89	2.93	299.1	20.7	2.26	14.03	67.77	0.14	17.73	85.67
BH	1.22	0.75	1.77	185.8	16.2	3.79	10.33	63.76	0.26	10.45	64.52

having similar nominal strength reinforcement ratio ($\rho_{nf, BF} = 1.94\% \approx \rho_{nf, BE} = 1.98\%$).

Table 6 presents the comparison of deflections under quasi-permanent moments combination, where FRP RC specimen BB is taken as a control specimen. $d_{q,BB}$ is the deflection corresponding to the quasi-permanent moments combination of control specimen BB (that is $M_{q, BB} = 10.37$ kN m). $M_{d,lim}$ is the moment corresponding to the deflection limit d_{lim}. $\eta_{d,u} = M_{d,lim}/M_u$ is the bending capacity utilization coefficient controlled by the deflection limit under serviceability state.

As observed from Table 6, the deflections of specimens with high nominal elastic modulus reinforcement ratio (specimens BA and BG) are less than the deflection limit under serviceability state. The deflection of steel and FRP RC specimens corresponding to the quasi-permanent moments combination of control specimen BB $d_{q,BB}$ is the smallest and largest, respectively; that of SFCB and hybrid reinforced specimens is between them; meanwhile, the deflection decreases with the increase in nominal elastic modulus reinforcement ratio. The bending capacity utilization coefficient controlled by the deflection limit under serviceability state $\eta_{d,u}$ of steel and FRP RC specimens is the highest and lowest, respectively, and that of SFCB and hybrid RC specimens is between them; meanwhile, the coefficient increases with the increase in nominal elastic modulus reinforcement ratio.
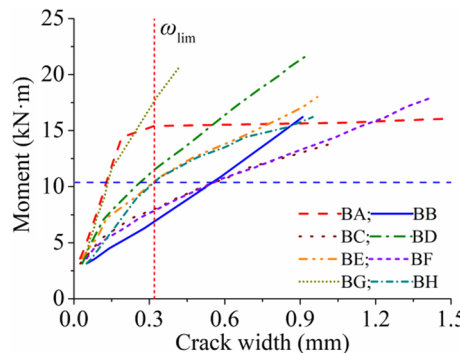
Fig. 10 Moment–crack width curves

3.3 Cracks and failure modes

Figure 10 presents the moment–crack width curves, where ω_{lim} is the crack width limit under serviceability state (that is 0.32 mm) [26, 31] for all specimens. Table 7 presents the comparison of crack widths under the quasi-permanent moments combinations, where FRP RC specimen BB is taken as a control specimen and $\omega_{q,BB}$ is the crack width corresponding to the quasi-permanent moments combination of control specimen BB. $M_{\omega,lim}$ is the moment corresponding to the crack width limit. $\eta_{\omega,u} = M_{\omega,lim}/M_u$ is the bending capacity utilization coefficient controlled by the crack width limit under serviceability state.

Table 7 Comparison of tested and predicted mechanical property of SFCB

No.	$f_{sfy,e}$	$f_{sfy,p}$	$f_{sfy,p}/f_{sfy,e}$	$E_{I,e}$	$E_{I,p}$	$E_{I,p}/E_{I,e}$	$f_{sfu,e}$	$f_{sfu,p}$	$f_{sfu,p}/f_{sfu,e}$	$E_{II,e}$	$E_{II,p}$	$E_{II,p}/E_{II,e}$
B	150.2	163.1	1.09	72.3	75.4	1.04	798.5	827.3	1.04	25.7	25.9	1.01
C	230.0	265.8	1.16	112.9	118.9	1.05	704.3	688.6	0.98	30.6	28.1	0.92
D	150.1	163.1	1.09	67.3	75.4	1.12	688.9	700.2	1.02	25.8	25.9	1.01
r_{mv}			1.11			1.07			1.01			0.95
r_{cov}			0.04			0.04			0.03			0.05

As observed from Table 7, the crack widths of specimens with high nominal elastic modulus reinforcement ratio (specimens BA,BD, BE, BG and BH) are less than the crack width limit under serviceability state. The crack width of steel and FRP RC specimens corresponding to the quasi-permanent moments combination of control specimen BB $\omega_{q,BB}$ is the smallest and largest, respectively; that of SFCB and hybrid RC specimens is between them; meanwhile, the crack width decreases with the increase in nominal elastic modulus reinforcement ratio. The bending capacity utilization coefficients controlled by the crack width limit under serviceability state $\eta_{\omega,u}$ of steel and FRP RC specimens are the highest and lowest, respectively, and those of SFCB and hybrid RC specimens are between them; meanwhile, the coefficients increase with the increase in nominal elastic modulus reinforcement ratio.

Figure 11 presents specimens' failure modes.

Typical appropriate reinforced flexural failure of concrete crushing occurred for all specimens. For steel RC specimen BA, as the steel reinforcement yielded, crack width and deflection significantly increased, until, finally, the top extreme concrete compressive fiber reached its ultimate strain and crushed. For SFCB RC specimens (BC, BD, BE and BF) and hybrid RC specimens (BG and BH), the development rates of crack width and deflection after yielding of steel also increase but at a slower rate compared with specimen BA as the external FRP wrapping was able to achieve a more stable behavior. However, as the load increased, the top extreme concrete compressive fiber reached its ultimate strain and crushed. For FRP RC specimen BB, the crack width and deflection were clearly larger than other specimens and eventually failed due to concrete crushing at the top extreme concrete compressive fiber. For all specimens, no signs of bond-slip occurred between the reinforcing bars and concrete.

4 Analysis of SFCB RC beams

4.1 Basic assumptions

4.1.1 Material constitutive model

(1) Concrete

The constitutive relationship of concrete [26] is shown in Fig. 12.

The compressive constitutive relationship of concrete can be represented by Eq. (1):

$$\sigma_c = \begin{cases} f_c\left(1 - \left(1 - \frac{\varepsilon_c}{\varepsilon_{co}}\right)^2\right), & 0 \le \varepsilon_c \le \varepsilon_{co} \\ f_c, & \varepsilon_{co} < \varepsilon_c \le \varepsilon_{cu} \end{cases} \quad (1)$$

where ε_c and σ_c are the compressive strain and corresponding stress in concrete, respectively; f_c is the concrete compressive strength; ε_{co} and ε_{cu} are the strain, while the stress up to compressive strength and the ultimate compressive strain, respectively.

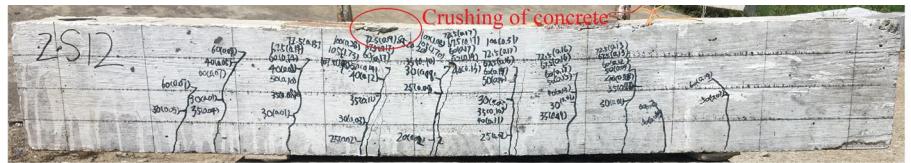The tensile constitutive relationship of concrete can be represented by Eq. (2):

$$\sigma_{ct} = \frac{f_{ctu}}{\varepsilon_{ctu}}\varepsilon_{ct}, \quad 0 \le \varepsilon_{ct} \le \varepsilon_{ctu} \quad (2)$$

where ε_{ct} and σ_{ct} are the tensile strain and corresponding stress in concrete, respectively, f_{ctu} and ε_{ctu} are the ultimate tensile strength and corresponding strain, respectively.
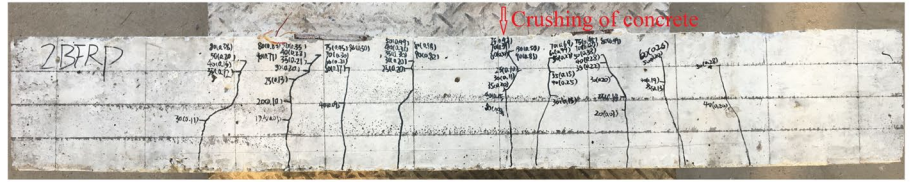
(2) SFCBs

Figure 13 represents the simplified tensile constitutive relationship [22] of SFCB. It can be expressed by Eq. (3), where ε_{sf} and σ_{sf} are the tensile strain and corresponding stress in SFCB material, E_I and E_{II} are the modulus of elasticity before and after yielding of inner steel, respectively, f_{sfy} and f_{sfu} are yield and ultimate strength, respectively, of SFCB, and ε_{sy} and σ_{fu} are yield strain of inner steel and ultimate tensile strain of out-wrapped FRP material, respectively.
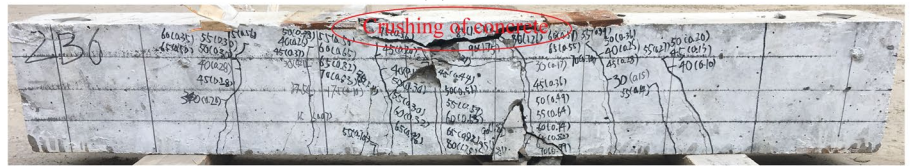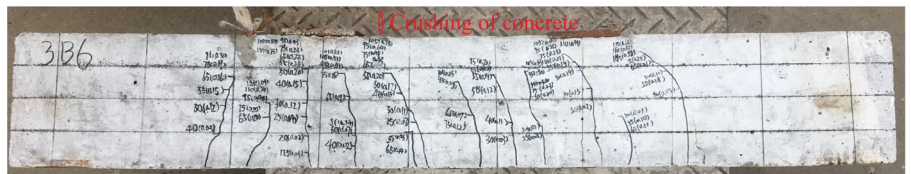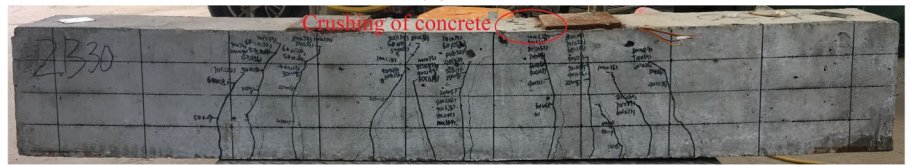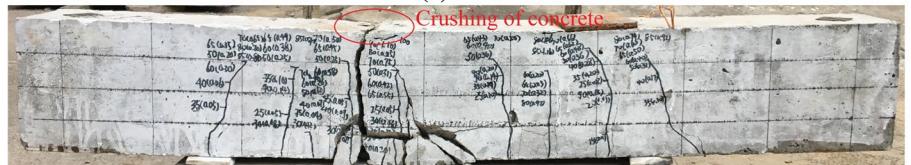
Fig. 11 Specimens' failure modes

(a) BA

(b) BB

(c) BC

(d) BD

(e) BE

(f) BF
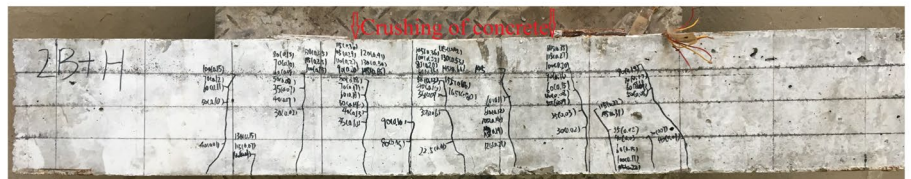
(g) BG
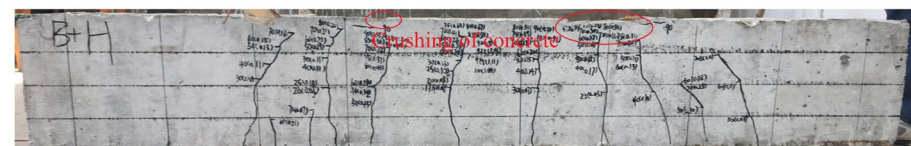
(h) BH

Fig. 12 Constitutive relationship of concrete

(a) Compression　　　　　　　　　　**(b)** Tension
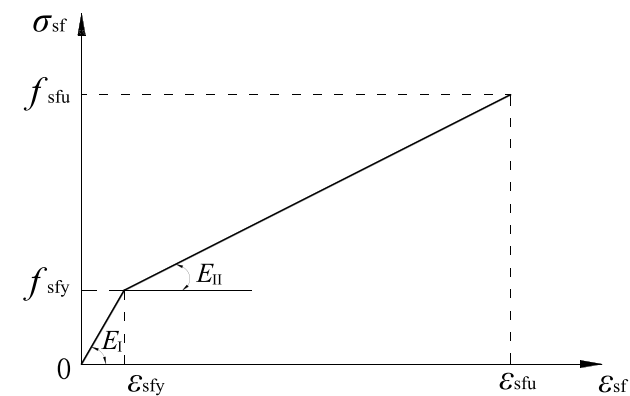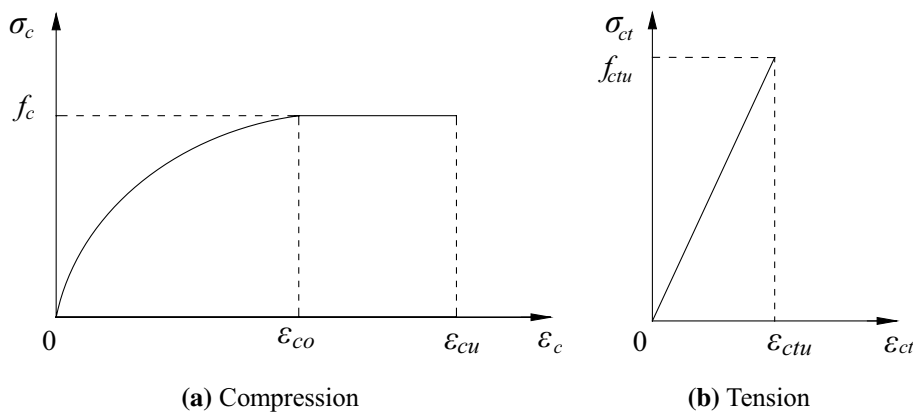
Fig. 13 Tensile constitutive relationship of SFCB

Fig. 14 Comparison of tested and predicted stress–strain curves

$$\sigma_{sf} = \begin{cases} E_I \varepsilon_{sf}, & 0 \leq \varepsilon_{sf} \leq \varepsilon_{sy} \\ f_{sfy} + E_{II}(\varepsilon_{sf} - \varepsilon_{sy}), & \varepsilon_{sy} < \varepsilon_{sf} \leq \varepsilon_{fu} \end{cases} \quad (3)$$

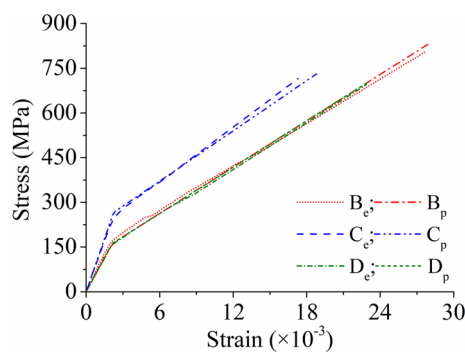According to the principle of composite materials, $E_I = a_s E_s + a_f E_f$, $E_{II} = a_f E_f$, where a_f and a_s are the cross section area ratio of out-wrapped FRP, A_f, and inner steel A_s cross section areas, respectively, to the total bar area A_{sf}, $a_f = A_f/A_{sf}$, $a_s = A_s/A_{sf}$.

A comparison of predicted and tested mechanical properties of SFCB is shown in Fig. 14 and Table 7, where the subscripts e and p represent the experimental and predicted values, respectively, r_{mv} and r_{cov} represent the mean value and coefficient of variation of the ratios of predicted value to experimental value, respectively.

As observed from Fig. 14 and Table 7, the predicted mechanical properties of SFCB show good agreement with that obtained from experiments.

4.1.2 Basic assumptions

The following assumptions have been taken into account in the analysis presented below:

- No slip occurs between SFCB/steel/FRP bars and surrounding concrete, i.e., perfect bond.
- The assumption of plane section at various loading stages is valid.
- The loading process of SFCB-reinforced flexural specimen exhibits three distinct stages as observed in experiments and described in Sect. 2.2, whereas failure occurs when either the extreme concrete compressive fiber or tensile SFCB reaches their respective ultimate strain.

4.2 Analysis of SFCB RC cross sections

4.2.1 Failure modes

Based on the materials' constitutive relationship, three failure modes and their corresponding strain distribution can be identified for SFCB-reinforced concrete specimens as shown in Fig. 15, where x_c and h_t are the height of compressive (neutral axis depth) and tensile concrete zone, respectively, and the subscripts 1 and 2 represent the balanced failure 1 and 2, respectively. h_0, h_r and h_0 are defined in Sect. 1.2, while ε_c, ε_{cu}, ε_{sfy}, ε_{sf} and ε_{sfu} are defined in Sect. 3.1. ① Compressive failure before SFCB reinforcement yielding (over-reinforced case): $\varepsilon_c = \varepsilon_{cu}$ and $\varepsilon_{sf} < \varepsilon_{sfy}$.
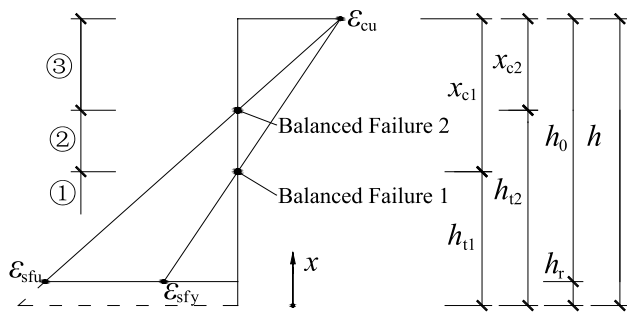
Fig. 15 Strain distribution under balanced failure modes

② Compressive failure 2 after yielding of SFCB: $\varepsilon_c = \varepsilon_{cu}$ and $\varepsilon_{sfy} \leq \varepsilon_{sf} < \varepsilon_{sfu}$. ③ Tensile failure: $\varepsilon_c < \varepsilon_{cu}$ and $\varepsilon_{sf} = \varepsilon_{sfu}$.

As presented in Fig. 15, if $\varepsilon_c = \varepsilon_{cu}$ and $\varepsilon_{sf} = \varepsilon_{sfy}$ simultaneously take place, balanced failure 1 occurs; if $\varepsilon_c = \varepsilon_{cu}$ and $\varepsilon_c = \varepsilon_{cu}$ simultaneously take place, balanced failure 2 occurs.

According to triangle similarity, the relative compression height ξ, which is defined as the depth of concrete compression zone x_c to the cross section effective height h_0, $\xi = x_c/h_0$, can be expressed as follows:

Balanced failure 1:

$$\xi_{cb1} = \frac{x_{c1}}{h_0} = \frac{\varepsilon_{cu}}{\varepsilon_{cu} + \varepsilon_{sfy}} \tag{4}$$

Balanced failure 2:

$$\xi_{cb2} = \frac{x_{c2}}{h_0} = \frac{\varepsilon_{cu}}{\varepsilon_{cu} + \varepsilon_{sfu}} \tag{5}$$

If $\xi > \xi_{cb1}$, failure mode ① occurs; if $\xi_{cb2} \leq \xi \leq \xi_{cb1}$, failure mode ② occurs; and if $\xi < \xi_{cb2}$, failure mode ③ occurs.

Considering equilibrium of compression force resisted by concrete and tensile force by SFCB, the following expression can be obtained:

$$\int_{h_t}^{h} \sigma_c(x)b\,\mathrm{d}x = \sigma_{sf}A_{sf} \tag{6}$$

where $\sigma_c(x)$ is the concrete compressive stress corresponding to the fiber at height x, A_{sf} and σ_{sf} are the SFCB cross-sectional area and tensile stress, respectively.

For balanced failure 1, $h_t = \varepsilon_{cu} h_0/(\varepsilon_{cu} + \varepsilon_{sfy})$.

$$f_c b h_0 \frac{\varepsilon_{cu} - \varepsilon_{co}/3}{\varepsilon_{cu} + \varepsilon_{sfy}} = f_{sfy}A_{sf} \tag{7}$$

Equation (7) can be transformed into the expression of reinforcement ratio, as follows:

$$\rho_{sf,b1} = \frac{f_c}{f_{sfy}} \cdot \frac{\varepsilon_{cu} - \varepsilon_{co}/3}{\varepsilon_{cu} + \varepsilon_{sfy}} \tag{8}$$

For balanced failure 2, $x_c = \varepsilon_{cu} h_0/(\varepsilon_{cu} + \varepsilon_{sfu})$.

$$f_c b h_0 \frac{\varepsilon_{cu} - \varepsilon_{co}/3}{\varepsilon_{cu} + \varepsilon_{sfy}} = f_{sfu}A_{sf} \tag{9}$$

Equation (9) can be transformed into the expression of reinforcement ratio, as follows:

$$\rho_{sf,b2} = \frac{f_c}{f_{sfu}} \cdot \frac{\varepsilon_{cu} - \varepsilon_{co}/3}{\varepsilon_{cu} + \varepsilon_{sfu}} \tag{10}$$

$\rho_{sf,b1}$ and $\rho_{sf,b2}$ are defined as the maximum and minimum balanced reinforcement ratio, respectively. So, if $\rho_{sf} > \rho_{sf,b1}$, failure mode ① occurs; if $\rho_{sf,b2} \leq \rho_{sf} \leq \rho_{sf,b1}$, failure mode ② occurs; if $\rho_{sf} < \rho_{sf,b2}$, failure mode ③ occurs.

4.2.2 Experimental verifications

The maximum and minimum balanced reinforcement ratios for SFCB RC specimens can be obtained from formulas (8) to (10). Comparisons of tested and predicted failure modes are presented in Table 8. CFM and EFM indicate the calculated and experimental failure modes, respectively. SY, SNY and CC indicate steel yielding, steel not yielded and concrete crushing, respectively.

As can be seen from Table 8, the predicted failure modes show good agreement with that observed in the experiments.

4.3 Section analysis of the whole loading process

Cross section analysis of the whole loading process of SFCB RC flexural specimens is developed. It is primarily based on materials' constitutive models, plane section assumption, triangle similarity and equilibrium of force. Figure 16a–e represents the diagrammatic sketches of cross section, strain

Table 8 Comparisons of experimental and predicted failure modes

No.	ρ_{sf} (%)	$\rho_{sf,b1}$ (%)	$\rho_{sf,b2}$ (%)	$\rho_{sf,b2} \leq \rho_{sf} \leq \rho_{sf,b1}$	CFM-ρ_{sf}	EFM
BC	1.22	7.64	0.41	Yes	②	SY, CC
BD	1.82	7.64	0.41	Yes	②	SY, CC
BE	1.22	4.63	0.33	Yes	②	SY, CC
BF	1.22	7.64	0.41	Yes	②	SY, CC
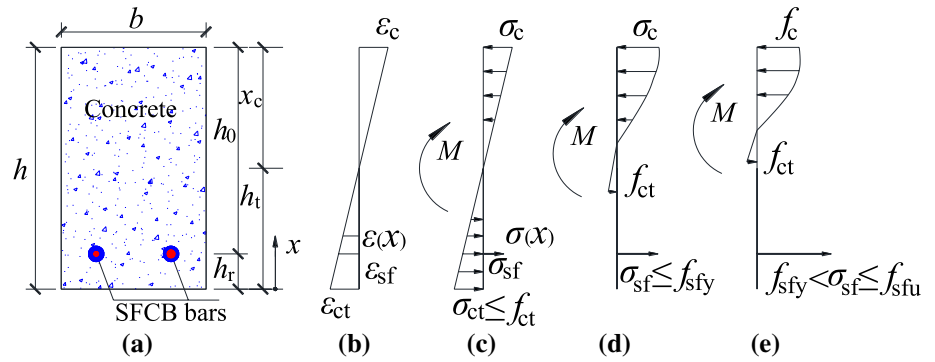
distribution and stress distribution of stages (I), (II) and (III), respectively.

4.3.1　Stage (I): elastic stage

In this stage, the strain in tensile concrete, SFCB and compressive concrete meets the following conditions: $0 < \varepsilon_{ct} \leq \varepsilon_{ctu}$, $0 < \varepsilon_{sf} < \varepsilon_{sfy}$ and $0 < \varepsilon_c < \varepsilon_{co}$, respectively.

The strain in the fiber at any height of cross section can be expressed as follows:

$$\varepsilon(x) = \begin{cases} \varepsilon_{ct}(h_t - x)/h_t, \ 0 \leq x \leq h_t \\ \varepsilon_{ct}(x - h_t)/h_t, \ h_t < x \leq h \end{cases} \quad (11)$$

The strain in the top outmost concrete fiber is $\varepsilon(h) = \varepsilon_{ct}(h - h_t)/h_t$, while the strain in SFCB reinforcement is $\varepsilon_{sf} = \varepsilon_{ct}(h_t - h_s)/h_t$ and the corresponding stress is $\sigma_{sf} = E_I \varepsilon_{ct}(h_t - h_s)/h_t$.

As the concrete compressive force is equal to the resultant tension of tensile concrete and SFCB, the following formula can be listed:

$$\int_0^{h_t} \sigma_{ct}(x)b dx + \sigma_{sf}A_{sf} - \int_{h_t}^h \sigma_c(x)b dx = 0 \quad (12)$$

Substituting Eq. (11) into Eq. (12), Eq. (12) can be converted to a function of h_t. By computer iterative calculation, h_t varying at loading stage (I) can be calculated. Taking the neutral axis as inertia axis, the cross section moment can be listed as follows:

$$M = \int_0^{h_t} \sigma_{ct}(x)b(h_t - x)dx + \sigma_{sf}A_{sf}(h_t - h_s) + \int_{h_t}^h \sigma_c(x)b(x - h_t)dx \quad (13)$$

When $\varepsilon_{ct} = \varepsilon_{ctu}$, cracking moment M_{cr} can be obtained by Eqs. (11) to Eq. (13).

4.3.2　Stage (II): from cracking of concrete to the yielding of SFCB

In this stage, the strain in tensile concrete, SFCB and compressive concrete meets the following conditions: $\varepsilon_{ct} > \varepsilon_{ctu}$, $0 < \varepsilon_{sf} \leq \varepsilon_{sfy}$ and $0 < \varepsilon_c \leq \varepsilon_{cu}$, respectively.

The strain of the fiber at any height of cross section can be conveyed as follows:

$$\varepsilon(x) = \begin{cases} \varepsilon_{sf}(h_t - x)/(h_t - h_s), \ 0 \leq x \leq h_t \\ \varepsilon_{sf}(x - h_t)/(h_t - h_s), \ h_t < x \leq h \end{cases} \quad (14)$$

The strain in the top outmost concrete fiber is $\varepsilon(h) = \varepsilon_{sf}(h - h_t)/(h_t - h_s)$. The strain and stress in SFCB are ε_{sf} and $\sigma_{sf} = E_I \varepsilon_{sf}$.

As the pressure bore by compressive concrete is equal to the tension bore by tensile SFCB, the following formula can be listed:

$$\sigma_{sf}A_{sf} - \int_{h_t}^h \sigma_c(x)b dx = 0 \quad (15)$$

Substituting Eq. (14) into Eq. (15), Eq. (15) can be converted to the function about h_t. By computer iterative calculation, h_t for varying loading at stage (II) can be calculated. Taking the neutral axis as inertia axis, the cross section moment is listed as follows:

$$M = \sigma_{sf}A_{sf}(h_t - h_s) + \int_{h_t}^h \sigma_c(x)b(x - h_t)dx \quad (16)$$

When $\varepsilon_{sf} = \varepsilon_{sfy}$, yield moment M_y can be obtained by Eq. (14) to Eq. (16).

4.3.3 Stage (III): from the yielding of SFCB to failure

In this stage, the strain in tensile concrete, SFCB and compressive concrete meets the following conditions: $\varepsilon_{ct} > \varepsilon_{ctu}$, $\varepsilon_{sfy} < \varepsilon_{sf} \leq \varepsilon_{sfu}$ and $0 < \varepsilon_c \leq \varepsilon_{cu}$, respectively.

The strain of the fiber at any height of cross section can be conveyed as follows:

$$\varepsilon(x) = \begin{cases} \varepsilon_c(h_t - x)/(h - h_t), \ 0 \leq x \leq h_t \\ \varepsilon_c(x - h_t)/(h - h_t), \ h_t < x \leq h \end{cases} \tag{17}$$

The strain in SFCB is $\varepsilon_{sf} = \varepsilon_c(h_t - h_s)/(h - h_s)$, and its corresponding stress is $\sigma_s = f_{sfy} + E_{II}(\varepsilon_{sf} - \varepsilon_{sfy})$.

Substituting Eq. (17) into Eq. (15), Eq. (15) can be converted to the function about h_t. By computer iterative calculation, h_t for varying loading at stage (III) can be calculated. The cross section moment can be obtained by Eq. (16).

When $\varepsilon_c = \varepsilon_{cu}$, ultimate moment M_u can be obtained by Eq. (15) to Eq. (17).

4.4 Comparisons of predicted and tested results

Comparisons of predicted cracking, yield and ultimate moment and tested results are presented in Table 9, where the subscripts e and p represent the experimental and predicted value, respectively, and r_{mv} and r_{cov} represent the mean value and coefficient of variation of ratios of predicted value to experimental value, respectively.

As observed from Table 9, the predicted bending capacity shows good agreement with tested results, illustrating the validity of the developed formulas.

5 Stiffness and deflection

For SFCB RC flexural specimens, after cracking, the test specimens exhibited two distinct flexural stiffnesses, before and after yielding of SFCB. So, the effective moment of inertia should be divided into two cases: I) before yielding of SFCB and II) after yielding of SFCB. I_g is the gross moment of inertia, $I_{e,\,I}$ and $I_{e,\,II}$ are the effective moment of inertia [30] before and after the yielding of SFCB, respectively. M, M_{cr} and M_y are the applied, cracking and yield moments, respectively. $I_{cr,\,I}$ and $I_{cr,\,II}$ are the cracked moment of inertia before and after, respectively, the yielding of SFCB. n_I and n_{II} are the modular ratio of SFCB before and after yielding, respectively, to concrete. k_I and k_{II} are the ratio of the height of concrete compressive zone before and after the yielding of SFCB, respectively, to effective height of cross section.

$$I_{e,I} = \left(\frac{M_{cr}}{M}\right)^3 I_g + \left[1 - \left(\frac{M_{cr}}{M}\right)^3\right] I_{cr,I} \leq I_g \tag{18}$$

$$I_{e,II} = \left(\frac{M_y}{M}\right)^3 I_y + \left[1 - \left(\frac{M_y}{M}\right)^3\right] I_{cr,II} \leq I_y \tag{19}$$

$$I_y = \left(\frac{M_{cr}}{M_y}\right)^3 I_g + \left[1 - \left(\frac{M_{cr}}{M_y}\right)^3\right] I_{cr,I} \tag{20}$$

$$I_{cr,I} = \frac{bh_0^3}{3}k_I^3 + n_{fI}A_{sf}h_0^2(1 - k_I)^2 \tag{21}$$

$$I_{cr,II} = \frac{bh_0^3}{3}k_{II}^3 + n_{fII}A_{sf}h_0^2(1 - k_{II})^2 \tag{22}$$

$$k_I = \sqrt{2\rho n_I + (\rho n_I)^2} - \rho n_I \tag{23}$$

$$k_{II} = \sqrt{2\rho n_{II} + (\rho n_{II})^2} - \rho n_{II} \tag{24}$$

If $M \leq M_{cr}$, $I_e = I_g$. If $M_{cr} < M \leq M_y$, the overall flexural stiffness $E_c I_{e,\,I}$ is between $E_c I_g$ and $I_{cr,\,I}$. If $M_y < M \leq M_u$, the overall flexural stiffness $E_c I_{e,\,II}$ is between $E_c I_y$ and $I_{cr,\,II}$.

The comparisons of predicted and tested moment–deflection curves of SFCB RC specimens are presented in Fig. 17.

Table 9 Comparison of tested and predicted moment capacity

Notation	BC	BD	BE	BF	r_{mv}	r_{cov}
$M_{cr,e}$ (kN m)	3.2	3.2	3.2	3.2	–	–
$M_{y,e}$ (kN m)	5.4	8.0	8.1	4.5	–	–
$M_{u,e}$ (kN m)	15.3	21.6	18.9	15.8	–	–
$M_{cr,p}$ (kN m)	3.03	2.83	3.34	3.00	–	–
$M_{y,p}$ (kN m)	5.5	8.1	8.4	4.4	–	–
$M_{u,p}$ (kN m)	14.5	21.8	17.9	18.1	–	–
$M_{cr,p}/M_{cr,e}$	0.96	0.90	1.06	0.95	0.97	0.07
$M_{y,p}/M_{y,e}$	1.02	1.00	1.05	0.98	1.01	0.03
$M_{u,p}/M_{u,e}$	0.95	1.01	0.95	1.15	1.01	0.09

Fig. 17 Comparison of predicted and tested moment–deflection curves

(a) BC

(b) BD

(c) BE

(d) BF
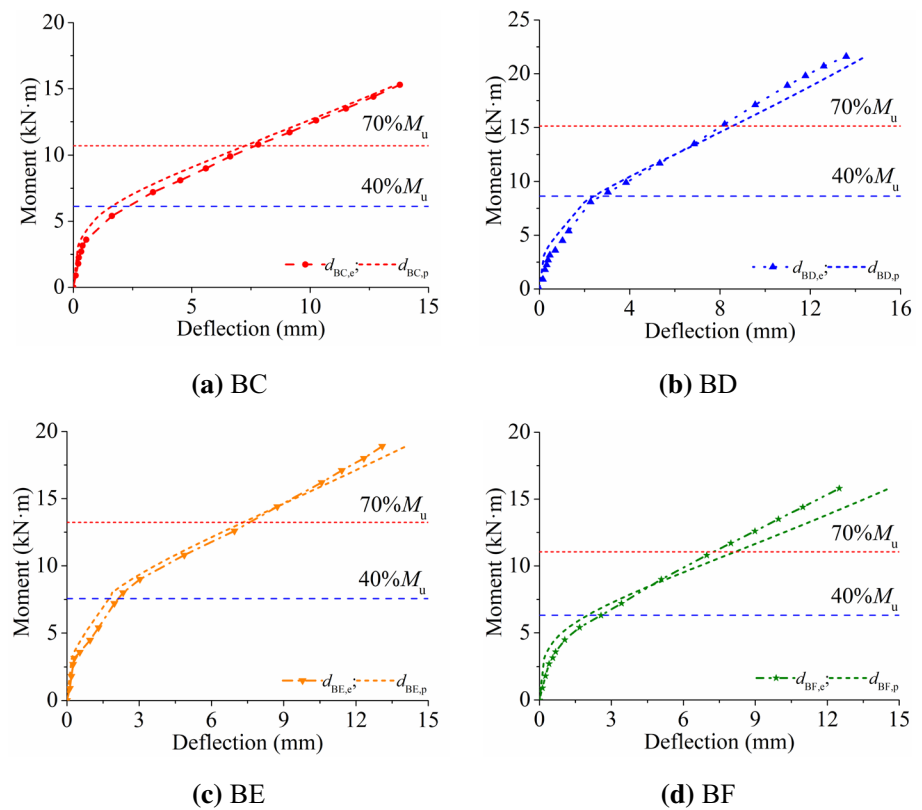
As observed from Fig. 17, the moment–deflection curves predicted by the modified formulas considering the mechanical properties of SFCB RC flexural specimens, especially under the service loading stage (about 40–70% bending capacity), fit well with the experimental results, confirming the validity of the developed formulas for practical use.

6 Crack width

The following formula is recommended by ACI 440.1R-06 [30] to predict the crack width of FRP RC flexural components:

$$w = 2\frac{f_f}{E_f}\beta k_d \sqrt{d_c^2 + s^2/4} \tag{25}$$

where w is the extreme crack width (the point at the tensile edge of cross section); f_f and E_f are the tensile stress and elastic modulus of FRP reinforcement, respectively; β is the ratio of the height of tensile zone to the distance between the neutral axis and centroid of reinforcement; k_b is a coefficient related to the bond property of reinforced bars and surrounding concrete; d_c is the concrete thickness of protective layer of FRP reinforcement, that is, the distance between the tensile edge of section and the centroid of FRP reinforcement; s is the spacing of reinforced bars.

For SFCB-reinforced concrete flexural specimens, the above formula for crack width is modified to Eq. (26) to account for mechanical characteristics of SFCB RC specimens as well as the location at which the crack width is calculated. The strain ε_{sf} in SFCB is calculated from Eq. (27):

$$w = 2\varepsilon_{sf}k_d \sqrt{d_c^2 + s^2/4} \tag{26}$$

$$\varepsilon_{sf} = \frac{M}{E_c I_e (1-k) h_0} \tag{27}$$

The comparisons of predicted and tested moment–crack width curves of SFCB RC specimens are presented in Fig. 18.

Figure 18 indicates that the moment–crack width curves predicted by the modified formulas show good agreement with tested results, especially under the service loading stage (about 40–70% bending capacity), illustrating the validity of the proposed formulas for engineering application.

7 Conclusions

Experimental and theoretical analyses of structural behavior of SFCB RC beams are carried out. The following conclusions may be drawn:

Fig. 18 Comparison of predicted and tested moment–crack width curves

(a) BC

(b) BD

(c) BE

(d) BF
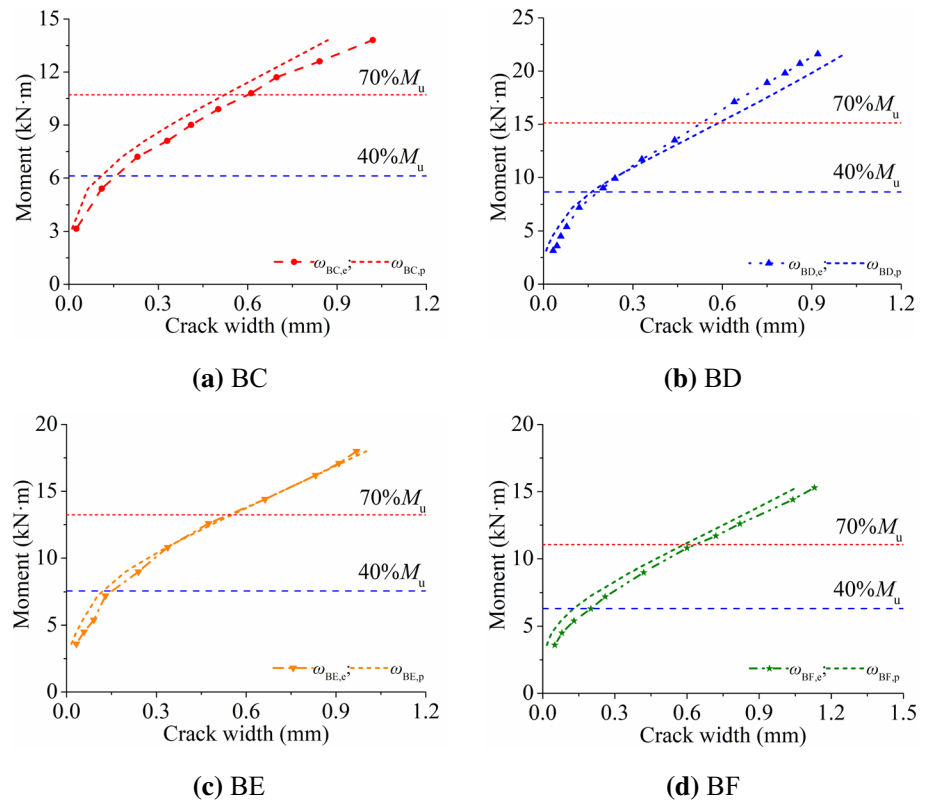
1. The predicted mechanical properties of SFCBs obtained by the principle of composite materials are in good agreement with the test results, and the ribbed SFCBs/BFRP bars showed comparable bond behavior to that of ribbed steel bars.

2. As SFCB has the characteristic of stable secondary stiffness, the loading processes of SFCB/hybrid RC specimens obviously present three stages. With an increase in nominal elastic modulus reinforcement ratio, the bending capacity increases gradually.

3. Deflections and crack widths of specimens with high nominal elastic modulus reinforcement ratio are less than the corresponding limits under serviceability state. Under the serviceability state, crack widths and deflections of steel and FRP RC specimens are the smallest and largest, respectively, while those of SFCB and hybrid RC specimens are in between; meanwhile, their values decrease with an increase in nominal elastic modulus reinforcement ratio.

4. For the bending capacity utilization coefficient controlled by the deflection/crack width limit under serviceability state, the values of steel and FRP RC specimens are the highest and lowest, respectively, while those of SFCB and hybrid RC specimens are between them and increase with the increase in nominal elastic modulus reinforcement ratio.

5. Based on strains compatibility, material's constitutive models and forces equilibrium, failure modes, balanced failure states and balanced reinforcement ratios as well as analytical technique for predicting the whole loading process are also developed, displaying good agreement with test results.

6. On the base of ACI design guidelines and taking the mechanical characteristics of SFCB RC beams into consideration, formulas for effective moment of inertia and crack width are proposed, showing good agreement with experimental results, illustrating their validity.

Compliance with ethical standards

Conflict of interest The authors declare that they have no conflict of interest.

References

1. Masmoudi R, Theriault M, Benmokrane B. Behavior of concrete beams reinforced with deformed fiber-reinforced plastic rods. ACI Struct J. 1998;95(6):665–75.
2. Grace NF, Sayed GA, Soliman AK, et al. Strengthening reinforced concrete beams under fiber-reinforced polymer (FRP) laminates. ACI Struct J. 1999;96(5):865–75.
3. Pecce M, Manfredi G, Cosenza E. Experimental response and code models of GFRP RC beams in bending. J Compos Constr. 2000;4(4):182–90.
4. Aiello MA, Ombres L. Load-deflection analysis of FRP-reinforced concrete flexural members. J Compos Constr. 2000;4(4):164–70.
5. Gravina RJ, Smith ST. Flexural behavior of indeterminate concrete beams reinforced with FRP bars. Eng Struct. 2008;30(9):2370–80.
6. Xue W, Zheng Q, Yang Y. Calculation method for deflection of concrete beams reinforced with FRP rebars. J Hydraul Eng. 2008;39(7):883–8.
7. Qi A, Weng C. Experiment Study on the mechanical behavior of continuous beams reinforced with FRP rebars. China Civ Eng J. 2008;41(5):2–7.
8. Tu Y, Zhang J, Qian Y, et al. Experimental and theoretical investigation of flexural load-carrying capacity of concrete beams reinforced with AFRP tendons. J Southeast Univ Nat Sci Ed. 2009;39(3):564–68.
9. Skuturna T, Valivonis J. The statistical evaluation of design methods of the load-carrying capacity of flexural reinforced concrete elements strengthened with FRP. Arch Civ Mech Eng. 2015;15(1):214–22.
10. Lapko A, Urbański M. Experimental and theoretical analysis of deflections of concrete beams reinforced with basalt rebar. Arch Civ Mech Eng. 2015;15(1):223–30.
11. Zhou D, Lei Z, Wang J. In-plane behavior of seismically damaged masonry walls repaired with external BFRP. Compos Struct. 2013;102:9–19.
12. Mahroug MEM, Ashour AF, Lam D. Experimental response and code modelling of continuous concrete slabs reinforced with BFRP bars. Compos Struct. 2014;107(1):664–74.
13. Lau D, Pam HJ. Experimental study of hybrid FRP reinforced concrete beams. Eng Struct. 2010;32:3857–65.
14. Huang H. Experimental study of steel-GFRP reinforced concrete beam. Shanghai: Tongji University; 2004.
15. Ge W-J, Ashour AF, Jiamin Yu, Gao P, Cao D-F, Cai C, Ji X. Flexural behavior of ECC-concrete hybrid composite beams reinforced with FRP and steel bars. J Compos Constr. 2019. https://doi.org/10.1061/(ASCE)CC.1943-5614.0000910.
16. Ge W, Zhang J, Cao D, Yongming T. Flexural behaviors of hybrid concrete beams reinforced with BFRP bars and steel bars. Constr Build Mater. 2015;87:28–37.
17. Kara IF, Ashour AF, Köroğlu MA. Flexural behavior of hybrid FRP/steel reinforced concrete beams. Compos Struct. 2015;129:111–21.
18. El Refai A, Abed F, Al-Rahmani A. Structural performance and serviceability of concrete beams reinforced with hybrid (GFRP and steel) bars. Constr Build Mater. 2015;96:518–29.
19. Yoo D-Y, Banthia N, Yoon Y-S. Flexural behavior of ultra-high-performance fiber-reinforced concrete beams reinforced with GFRP and steel rebars. Eng Struct. 2016;111:246–62.
20. Sun Z, Fu L, Feng DC, Vatuloka AR, Wei Y, Wu G. Experimental study on the flexural behavior of concrete beams reinforced with bundled hybrid steel/FRP bars. Eng Struct. 2019;197:109443.
21. Maranan G, Manalo A, Benmokrane B, Karunasena WM, Mendis P, Nguyen KTQ. Flexural behavior of geopolymer-concrete beams longitudinally reinforced with GFRP and steel hybrid reinforcements. Eng Struct. 2019;182:141–52.
22. Gang W, Zhi-Shen W, Luo Y-B, Sun Z-Y, Xian-Qi H. Mechanical properties of steel-FRP composite bar under uniaxial and cyclic tensile loads. J Mater Civ Eng. 2010;22(10):1056–66.
23. Sun ZY, Wu G, Zhang J, Zeng YH, Xiao W. Experimental study on concrete columns reinforced by hybrid steel-fiber reinforced polymer (FRP) bars under horizontal cyclic loading. Constr Build Mater. 2017;130:202–11.
24. Sun ZY, Yang Y, Yan W, Wu G, He X. Moment curvature behaviors of concrete beams singly reinforced by steel-FRP composite bars. Adv Civ Eng. 2017. https://doi.org/10.1155/2017/1309629.
25. China Academy of Building Research. GB/T50081-2016: standard for test method of mechanical properties on ordinary concrete. Beijing: China Building Industry Press; 2016.
26. China Academy of Building Research. Code for design of concrete structures GB50010-2010. Beijing: China Building Industry Press; 2010.
27. American Concrete Institute. Guide test methods for fiber-reinforced polymers (FRPs) for reinforcing or strengthening concrete structures ACI 440.3R-04. Farmington Hills: American Concrete Institute; 2004.
28. China Academy of Building Research. Standard for test method of concrete structures GB 50152-2012. Beijing: China Building Industry Press; 2012.
29. Wang CZ, Teng ZM. Theory of Concrete Structure. Beijing: China Building Industry Press; 1983. p. 278.
30. American Concrete Institute. ACI 440.1R-06: Guide for the design and construction of structural concrete reinforced with FRP bars. Farmington Hills: American Concrete Institute; 2006.
31. American Concrete Institute. ACI 224R-01: Control of cracking in concrete structures. Farmington Hills: American Concrete Institute; 2001.